

NASA Technical Paper 1110

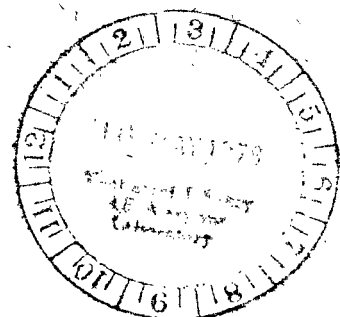
LOAN COPY: RETURN TO
AFWL TECHNICAL LIBRARY
KIRTLAND AFB, N. M.



In-Place Recalibration Technique Applied to a Capacitance-Type System for Measuring Rotor Blade Tip Clearance

John P. Barranger

APRIL 1978





NASA Technical Paper 1110

In-Place Recalibration Technique Applied to a Capacitance-Type System for Measuring Rotor Blade Tip Clearance

John P. Barranger
*Lewis Research Center
Cleveland, Ohio*



National Aeronautics
and Space Administration

**Scientific and Technical
Information Office**

1978

IN-PLACE RECALIBRATION TECHNIQUE APPLIED TO A CAPACITANCE-TYPE SYSTEM FOR MEASURING ROTOR BLADE TIP CLEARANCE

by John P. Barranger
Lewis Research Center

SUMMARY

The rotor-blade-tip clearance measurement system consists of a capacitance-sensing probe with self-contained tuning elements, a connecting coaxial cable, and remotely located electronics. Using complex variable and electrical network theory, equations are derived that characterize the system operation. The quantities that determine the accuracy of the system are strong functions of probe tip temperature and humidity and therefore depend on the environment at the probe tip during the normal operation. A novel in-place recalibration technique is presented which partly overcomes this problem through a simple modification of the electronics that permits a scale-factor correction. The quantities that determine the scale factor are measured during calibration and during the normal operation, that is, during in-place recalibration.

The in-place recalibration technique is applied to a commercial system under conditions of 5 to 95 percent relative humidity and temperatures up to 370°C (700°F). Over the clearance range of 0 to 1000 micrometers (40 mils), the recalibration technique reduced the errors caused by changes in humidity from a maximum of 45 micrometers (1.8 mils) to a maximum of 10 micrometers (0.4 mil) and reduced the errors caused by temperature from a maximum of 88 micrometers (3.5 mils) to a maximum of 40 micrometers (1.6 mils).

Equations are also found that characterize the important cable and probe design quantities. It is shown that under certain circumstances mutual inductive tuning of the probe may be necessary.

INTRODUCTION

The long need for jet engine rotor-blade-tip-clearance measurement devices has been intensified recently by advances in technology. Advanced engine designs encompass lightweight, high-performance concepts such as the use of small, thin airfoils for

blades and tighter running clearances to achieve improved fuel efficiency.

Capacitance sensors are used extensively for the measurement of rotor-blade-tip clearance. The capacitance principle has also been applied to pressure transducers, accelerometers, and in biological activity monitoring.

In this report a novel in-place recalibration technique is applied to a capacitance type of rotor-blade-tip-clearance measurement system. The system consists of a capacitance-sensing probe with self-contained tuning elements, a connecting coaxial cable, and remotely located electronics. Using complex variable and electrical network theory, equations are derived that characterize the system operation. The quantities that determine the accuracy of the system are strong functions of probe tip temperature and humidity and therefore depend on the environment at the probe tip during the normal operation. The in-place recalibration technique partly overcomes this problem through a simple modification of the electronics that permits a scale-factor correction. Calibration and in-place recalibration methods of measurement for the quantities that determine the scale factor are also described.

The in-place recalibration technique is applied to the commercial system under conditions of 5 to 95 percent relative humidity and temperatures to 370°C (700°F). Over the clearance range of 0 to 1000 micrometers (40 mils), the recalibration technique reduced the errors caused by changes in humidity from a maximum of 45 micrometers (1.8 mils) to a maximum of 10 micrometers (0.4 mil) and reduced the errors caused by temperature from a maximum of 88 micrometers (3.5 mils) to a maximum of 40 micrometers (1.6 mils).

The equations in appendix A characterize the important cable and probe design quantities. It is shown that under certain circumstances mutual inductive tuning of the probe may be necessary. Appendix B is a list of symbols used in this report.

SYSTEM THEORY OF OPERATION AND METHODS OF MEASUREMENT

This section is divided into three subsections. In the first subsection, using circuit theory and the theory of functions of complex variables, equations are derived that characterize the system operation. The quantities that determine the accuracy of the system are strong functions of probe tip temperature and humidity and therefore depend on the environment at the probe tip during normal operation. In the second subsection the in-place recalibrated technique partly overcomes the above problem through a simple modification of the electronics that permits a scale-factor correction. In the last subsection calibration and in-place recalibration methods of measurement for the quantities that determine the scale factor are described.

System Quantities

Figure 1 is a schematic of a rotor blade and the probe tip of a typical shroud-mounted capacitance-sensing probe. The probe tip has a rigid coaxial construction, that is, a solid inner conductor separated from a solid outer tube by an insulator. As the blade passes under the probe tip, the capacitance between the inner conductor and the blade tip is a measure of the distance between them.

The equivalent admittance, as seen from the terminal pair 2-2', can be considered the parallel combination of a capacitance and a shunt resistance. Let the shunt resistance be designated R_c . The capacitance is the sum of the capacitance of the coaxial probe tip alone and the inner conductor to blade tip capacitance. Let this total capacitance at the point of maximum capacitance be denoted by

$$C_m = C_o + C(d) \quad (1)$$

where C_o is the coaxial probe tip capacitance, $C(d)$ is the blade capacitance, and d is the distance between the inner conductor and the blade tip. Blade capacitance $C(d)$ increases as d decreases and is a function of the geometries of the probe tip and blade as well.

Figure 2 shows $C(t)$, the capacitance as a function of time, for the passing of two blades under the probe tip. The probe tip diameter is usually made much smaller than the interblade spacing. For this reason $C(t)$ equals C_o between blade pairs. The blade capacitance $C(d)$ is the difference between the maximum and the minimum capacitance, that is, $C_m - C_o$.

The values of C_o and of the shunt resistance R_c depend on the geometry of the coaxial probe tip and the electrical characteristics of the insulator. It is known that the dielectric properties of an insulator change with temperature. Further, the electrical characteristics of exposed insulator surfaces are subject to changes in humidity. The quantities C_o and R_c are therefore influenced by the temperature of the insulator and the humidity in the space around the probe tip.

The value of $C(d)$ is usually small compared with that of C_o , of the order of 2 to 10 percent. Furthermore, the coaxial cable that connects the probe and the electronic equipment has its own reactance elements which add to C_o . Moreover, the inevitable motion and vibration of the cable causes changes in the cable reactance elements that are frequently larger in equivalent magnitude than $C(d)$. To overcome these difficulties, the admittance as seen from terminal pair 2-2' of figure 1 is made part of a tuned circuit with self-contained tuning elements rigidly mounted as an integral part of the probe. As is shown in a later section, this approach magnifies the value of $C(d)$ and minimizes system dependency on changes in coaxial cable parameters.

Figure 3 is a system block diagram showing the electronics, cable, probe, and

rotor. The system electrical equivalent circuit is illustrated in figure 4. The electronics consist of a source of radiofrequency voltage e_g of angular frequency ω in series with its source admittance y_g and an amplitude detector A for measuring the magnitude of the voltage e . The network N represents the cable and probe tuning elements and has an input admittance y when loaded by C and R_c , the total capacitance and shunt resistance, respectively. In the following paragraphs it is shown that the change in the magnitude of e is a measure of the change in capacitance $C(d)$ and therefore is also a measure of the clearance d .

Using conventional circuit analysis, the voltage e is given by

$$e = \frac{e_g y_g}{y + y_g} \quad (2)$$

where all the quantities are complex functions of the variable $j\omega$. The input admittance of A is designed to be very much smaller than y . The voltage e is a function of both C and R_c , since e is a function of y and y , in turn is a function of C and R_c . As is shown in a later section, the influence of R_c is minor compared with that of C . Denoting e_c as the voltage e when C is changed, the differential given by

$$e_{cm} - e_{co} = \left(\frac{de}{dC} \right)_o \cdot (C_m - C_o) = \left(\frac{de}{dC} \right)_o \cdot \Delta C \quad (3)$$

defines a linear approximation of e_c . As is shown later in this section, a certain type of nonlinearity is permitted without changing the results. The positive quantity $(C_m - C_o) = \Delta C$ is the change in capacitance $C(d)$ as a result of the passing of a blade under the probe tip. (See fig. 2.) The quantity $e_{cm} - e_{co}$ is the corresponding change of the voltage e_c . The factor $(de/dC)_o$ is the derivative of e with respect to C , evaluated at $C = C_o$. The operating range of C_o includes changes in C_o due to variations in temperature and humidity. The derivative de/dC in equation (3) exists because the network is physically real and passive and therefore is analytic in the vicinity of $C = C_o$.

Equating the magnitude of each side of equation (3) yields the expression

$$|e_{cm} - e_{co}| = \left| \left(\frac{de}{dC} \right)_o \right| \cdot \Delta C \quad (4)$$

It is now assumed that the phase angle of e and, therefore, of e_c do not change with C over the range of C , which includes the operating range of C_o and all ΔC . This

approximation is verified in a later section where for a commercial system it is shown that the phase angle of e changes by less than 4° . Thus

$$|e_{cm} - e_{co}| = |e_{cm}| - |e_{co}| = \Delta |e_c|$$

where $\Delta |e_c|$ is the change in the magnitude of e_c . Equation (4) now becomes

$$\Delta |e_c| = \left| \left(\frac{de}{dC} \right)_0 \right| \cdot \Delta C \quad (5)$$

Equation (5) states that if the magnitude of the derivative is known, the change in the magnitude of e_c is a measure of ΔC and, therefore, is also a measure of the clearance d .

The quantity $\Delta |e_c|$ is found by taking the difference between the maximum and minimum output of the amplitude detector A as the blade passes under the probe tip. The quantity $\left| \left(\frac{de}{dC} \right)_0 \right|$ is a strong function of C_0 and depends on temperature and humidity. As is shown in a later section the magnitude of $\left(\frac{de}{dC} \right)_0$ changes by 14 percent. It can be measured during calibration, but it is difficult to determine under operating conditions since the temperature and humidity are not usually known in the vicinity of the probe tip. Thus the varying nature of $\left(\frac{de}{dC} \right)_0$ results in errors in the clearance measurements.

To overcome this difficulty, equation (3) is modified in such a way that the significant quantities are either measurable or constant. To show this, first the function-of-function rule is applied to de/dC , that is,

$$\frac{de}{dC} = \frac{de}{dy} \cdot \frac{dy}{dC}$$

Then, by following this procedure, equation (3) becomes

$$e_{cm} - e_{co} = \left(\frac{de}{dy} \right)_0 \cdot \left(\frac{dy}{dC} \right)_0 \cdot \Delta C \quad (6)$$

where the factor $\left(\frac{dy}{dC} \right)_0$ is the derivative of y with respect to C evaluated at $C = C_0$, and the factor $\left(\frac{de}{dy} \right)_0$ is the derivative of e with respect to y , evaluated at $C = C_0$. Equating the magnitude of each side, equation (6) becomes

$$\Delta |e_c| = \left| \left(\frac{de}{dy} \right)_0 \right| \cdot \left| \left(\frac{dy}{dC} \right)_0 \right| \cdot \Delta C \quad (7)$$

The quantity $|(de/dy)_0|$ is a strong function of C_0 . The in-place recalibration technique described later in this section provides a method for its measurement over the operating range of C_0 . The other quantity $|(dy/dC)_0|$ is fortunately a weak function of C_0 . It is measured as part of the calibration and is assumed unchanged over the operating range of C_0 . This approximation is verified in a later section where it is shown that $|(dy/dC)_0|$ changes by only 3 percent. Thus, the highly variable and unmanageable quantity $|(de/dC)_0|$ has been replaced by the product of a still highly variable but now measureable factor $|(de/dy)_0|$ and the constant factor $|(dy/dC)_0|$.

In-Place Recalibration

In this subsection it is shown that the in-place recalibration technique provides a method of measuring the value of $|(de/dy)_0|$ in equation (7) during the time the system is in use, that is, over the operating range of C_0 . This is done through a simple modification of the electronics that permits the determination of the quantities for the scale-factor correction. Measurements of the quantities are made during calibration and during in-place recalibration.

Figure 5 shows the system equivalent circuit with in-place recalibration. The switch K and the admittance y_k have been added to the electronics portion of the system. With the switch K closed, y is the parallel combination of y_k and the input admittance of N.

It should be noted that in the conventional in-place recalibration technique (ref. 1), the parallel admittance is connected directly across the sensing element, in this case the capacitance C in figure 5. However, because of the small value of capacitance change and the uncertain stray capacitances, an accurate and stable parallel admittance is not practical. The novel placement of y_k away from the sensing element minimizes these problems while maintaining the usefulness of the method. Another disadvantage of the conventional technique is the usual requirement for both magnitude and phase-angle measurements. Thus, another simplifying and novel feature of figure 5 is the measurement only of the magnitude of e by amplitude detector A and not its phase angle.

Using an argument similar to the one used previously, a relationship is found between the change in the magnitude of e and the change in the magnitude of y when K is changed from the open to the closed position. For $C = C_0$ let y be denoted by

$$y_n = y_0 + y_k$$

where y_0 is the input admittance of N with the switch K open. This equation is similar to equation (1). Since e is a function of y the differential given by

$$e_{yn} - e_{yo} = \left(\frac{de}{dy} \right)_o \cdot (y_n - y_o) = \left(\frac{de}{dy} \right)_o \cdot y_k \quad (8)$$

defines a linear approximation of e_y where e_y is the voltage e when y is changed. The quantity $(y_n - y_o) = y_k$ is the change in admittance resulting from switch closure. The quantity $e_{yn} - e_{yo}$ is the corresponding change of the voltage e_y . Equation (8) is similar to equation (6). Equating the magnitude of each side of equation (8) yields the expression

$$|e_{yn} - e_{yo}| = \left| \left(\frac{de}{dy} \right)_o \right| \cdot |y_k| \quad (9)$$

For equation (6) it is now assumed that the phase angle of $(dy/dC)_o$ does not change with C over the operating range of C_o . This approximation is verified in a later section where it is shown that the phase angle of $(dy/dC)_o$ changes by less than 2° . Further, let the phase angle of y_k equal the phase angle of $(dy/dC)_o$. Since $e_{yo} = e_{co}$ and the phase angle of e_{yn} is now the same as the phase angle of e_{cm} , the phase angle of e_y does not change with C over the range of C , which includes the operating range of C_o and all ΔC . Thus

$$|e_{yn} - e_{yo}| = |e_{yn}| - |e_{yo}| = \Delta |e_y|$$

where $\Delta |e_y|$ is the change in the magnitude of e_y . Equation (9) now becomes

$$\Delta |e_y| = \left| \left(\frac{de}{dy} \right)_o \right| \cdot |y_k| \quad (10)$$

From equation (10) it can be seen that since y_k is fixed, $\Delta |e_y|$ is a measure of $\left| \left(\frac{de}{dy} \right)_o \right|$. Thus, long-term variations in the magnitude of the derivative due to changes in C_o are reflected in changes in $\Delta |e_y|$.

It is desirable that the amplitude detector A measure both $\Delta |e_y|$ and $\Delta |e_o|$ on the same scale, that is, that these quantities be of the same order of magnitude. Comparison of equations (7) and (10) shows that this can be achieved at approximately one-half scale if

$$|y_k| \approx \left| \left(\frac{dy}{dC} \right)_o \right| \cdot \frac{(\Delta C)_m}{2} \quad (11)$$

where $(\Delta C)_m$ is the maximum expected ΔC . Thus the value of y_k is now completely

determined since its magnitude is given by equation (11) and its phase angle is equal to the phase angle of $(dy/dC)_o$.

It is now shown that measurements of $\Delta|e_y|$ determine the scale factor that can be used to correct the data taken during calibration. The measurement procedure is as follows: (1) A single value of $\Delta|e_y|$ is measured during routine calibration where $\Delta|e_c|$ is determined over the required range of clearance d . (2) The value of $\Delta|e_y|$ is measured again in place, that is, with the probe mounted in the desired location and the system in the normal operational condition. And (3) the values of the two $\Delta|e_y|$'s measured under steps (1) and (2) are used to scale $\Delta|e_c|$, and the resultant quantity is applied to the calibration curve derived in (1) to determine the clearance.

For the purpose of detailing the formulation, let $\Delta|e_{ca}|$ be $\Delta|e_c|$ for the calibration condition measured in step (1). Equation (7) can be written as

$$\Delta|e_{ca}| = \left| \left(\frac{de}{dy} \right)_{oa} \right| \cdot \left| \left(\frac{dy}{dC} \right)_{oa} \right| \cdot \Delta C \quad (12)$$

where the derivatives are evaluated at C_{oa} , the probe capacitance at the time of calibration. The environmental conditions are such that the value of C_{oa} is usually stable during calibration. Further, let $\Delta|e_{ya}|$ be the value of $\Delta|e_y|$ for the calibration condition. Equation (10) can then be written as

$$\Delta|e_{ya}| = \left| \left(\frac{de}{dy} \right)_{oa} \right| \cdot |y_k| \quad (13)$$

Equation (12) becomes, after eliminating the derivative $(de/dy)_{oa}$ from equations (12) and (13),

$$\Delta|e_{ca}| = \frac{\Delta|e_{ya}|}{|y_k|} \cdot \left| \left(\frac{dy}{dC} \right)_{oa} \right| \cdot \Delta C \quad (14)$$

Let $\Delta|e_{cb}|$ be $\Delta|e_c|$ for the operational condition. Equation (7) is now

$$\Delta|e_{cb}| = \left| \left(\frac{de}{dy} \right)_{ob} \right| \cdot \left| \left(\frac{dy}{dC} \right)_{ob} \right| \cdot \Delta C \quad (15)$$

where the derivatives are evaluated at C_{ob} , the probe capacitance existing during the operational condition. The environmental conditions are such that the value of C_{ob} is usually stable during the measurement time, normally less than 10 seconds. Further, let $\Delta|e_{yb}|$ be the value of $\Delta|e_y|$ for this condition. Equation (10) is now

$$\Delta |e_{yb}| = \left| \left(\frac{de}{dy} \right)_{ob} \right| \cdot |y_k| \quad (16)$$

and equation (15) becomes

$$\Delta |e_{cb}| = \frac{\Delta |e_{yb}|}{|y_k|} \cdot \left| \left(\frac{dy}{dC} \right)_{ob} \right| \cdot \Delta C \quad (17)$$

After eliminating $\Delta C/|y_k|$ from equations (14) and (17), equation (14) becomes

$$\Delta |e_{ca}| = \Delta |e_{cb}| \cdot \frac{\Delta |e_{ya}|}{\Delta |e_{yb}|} \cdot \frac{|(dy/dC)_{oa}|}{|(dy/dC)_{ob}|} \quad (18)$$

By the previous assumption presented with equation (7), $|(dy/dC)_o|$ is constant with C over the operating range of C_o , including, of course, the values of C_{oa} and C_{ob} . Setting the last factor of equation (18) to unity, equation (18) becomes

$$\Delta |e_{ca}| = \Delta |e_{cb}| \cdot \frac{\Delta |e_{ya}|}{\Delta |e_{yb}|} \quad (19)$$

Equation (19) is the desired equation showing the in-place recalibration achieved through the correction of $\Delta |e_{cb}|$ by a scale factor which is the ratio of the value of $\Delta |e_{ya}|$ measured during calibration and the value of $\Delta |e_{yb}|$ measured under the actual operational condition. The clearance is obtained by applying equation (19) to the calibration curve obtained in step (1).

This analysis depends on the linear approximations of equations (3) and (8). It should be noted that a certain type of nonlinearity is permitted without changing the results. Let the approximation

$$e_{cm} - e_{co} = \left(\frac{de}{dC} \right)_o \cdot (C_m - C_o) \cdot \left[1 + K_{1C}(C_m - C_o) + K_{2C}(C_m - C_o)^2 + \dots \right] \quad (20)$$

and the approximation

$$e_{yn} - e_{yo} = \left(\frac{de}{dy} \right)_o \cdot (y_n - y_o) \cdot \left[1 + K_{1y}(y_n - y_o) + K_{2y}(y_n - y_o)^2 + \dots \right] \quad (21)$$

where none of the K 's are functions of C_o , be substituted for equations (3) and (8), respectively. By following an identical procedure, it can be shown that the bracketed factors of equations (20) and (21) are eliminated and the final result, equation (19), is unchanged. Thus the in-place recalibration technique can be applied to calibration curves that follow this type of nonlinearity, that is, where the K 's are not functions of C_o .

Methods of Measurement

Calibration and in-place recalibration methods of measurement for the quantities $\Delta|e_{ya}|$ and $\Delta|e_{yb}|$ that determine the scale factor are now described. The other quantities of interest in equation (19), $\Delta|e_{ca}|$ and $\Delta|e_{cb}|$ are also discussed.

Figure 6 is a block diagram of the calibration system. The probe is mounted to a plate which simulates the shroud. A precision, bidirectional table is used to translate the mounted blade in the two directions indicated in the figure. Movement parallel to the plate simulates rotor blade motion, while motion perpendicular to the plate is used to set the clearance d .

During calibration the desired clearance is set and then the mounted blade is moved parallel to the plate beginning and ending at simulated interblade positions. The output of the amplitude detector is at first a constant then increases as the probe is approached, reaches a peak, then decreases as the blade moves away from the probe and finally levels out again. Figure 7 shows the output wave form during calibration. The quantity $\Delta|e_{ca}|$ is found by taking the difference between the maximum and minimum output as the blade passes under the probe tip. The plot of $\Delta|e_{ca}|$ as a function of d is the calibration curve. The single quantity $\Delta|e_{ya}|$ is the change in the output when the switch K is closed while the blade is stationary at the interblade position.

Under the normal operational condition, the amplitude detector output is a series of waveforms, each corresponding to a blade passing under the probe tip. Figure 7 shows this output during in-place recalibration. The quantity $\Delta|e_{cb}|$ for any given blade is found by taking the difference between the maximum and minimum output as that blade passes under the probe tip. The quantity $\Delta|e_{yb}|$ is the change in the output when switch K is closed. This measurement is made at the interblade positions before and after the switch closure, as illustrated in figure 7. The dashed lines represent the transient that occurs immediately after the switch is closed. If the environmental conditions in the vicinity of the probe tip change during the system's normal operation, these measurements are repeated to obtain updated values of $\Delta|e_{cb}|$ and $\Delta|e_{yb}|$.

The quantities $\Delta|e_{cb}|$, $\Delta|e_{ya}|$, and $\Delta|e_{yb}|$ are used in equation (19) to solve for $\Delta|e_{ca}|$. The clearance is obtained by finding the d corresponding to $\Delta|e_{ca}|$ on the calibration curve.

The important approximations used in the derivation of the in-place recalibration equation (19) are as follows:

(1) Equations (3) and (8) (or (20) and (21)) are valid approximations of e_c and e_y , respectively.

(2) The phase angle of e does not change with C over the range of C , which includes the operating range of C_o and all ΔC .

(3) The magnitude and phase angle of $(dy/dC)_o$ do not change with C over the operating range of C_o .

It is clear that the design of an appropriate system should be optimized with respect to these factors. In the following sections it is shown that an unoptimized commercial measurement system sufficiently approximates the conditions to yield useful results.

SYSTEM ANALYSIS

In this section a commercial system consisting of electronics, connecting coaxial cable, and probe network is analyzed. Component values of the network elements are inserted in the equations and the resultant calculations of magnitude and phase angle of e and y , and the magnitudes of $(de/dC)_o$ and $(dy/dC)_o$ are plotted as functions of capacitance. The calculations show that

(1) The presence of the shunt resistance R_c across C in the equivalent circuit has only minor influence on the plotted curves.

(2) The phase angle of e changes by less than 4° over the range of C , which includes the operating range of C_o and all ΔC .

(3) The magnitude of $(de/dC)_o$ is a strong function of C , changing by 14 percent over the operating range of C_o .

(4) The magnitude of $(dy/dC)_o$ is a weaker function of C , changing by only 3 percent over the operating range of C_o .

(5) The phase angle of $(dy/dC)_o$ changes by less than 2° over the operating range of C_o .

(6) The tuning elements cause y to be a sensitive indicator of clearance by magnifying the value of $C(d)$ by a factor of approximately 240.

The system equivalent circuit consisting of the electronics, the connecting coaxial cable, and a probe network is shown in figure 8. It is the same as figure 5 except that network N has been separated into two networks, N_1 and N_2 . Network N_2 represents the probe-tuning elements and has an input admittance of y_p when loaded by C and R_c . Network N_1 represents the cable and with K open has an input admittance of y when loaded by y_p .

From transmission line theory (ref. 2) it is known that

$$y = \frac{1}{Z_0} \left[\frac{y_p Z_0 + \tanh(\alpha + j\beta)l}{1 + y_p Z_0 \tanh(\alpha + j\beta)l} \right] \quad (22)$$

where Z_0 is the characteristic impedance, α is the attenuation constant, β is the phase constant and l is the length of the line. The quantities Z_0 , α , and β are characteristic of the particular type of coaxial cable used.

It was found experimentally that the circuit of figure 9 represents the probe network N_2 loaded by C and R_c . The equations that characterize the important design quantities for this network and the cable are derived in appendix A. The input admittance of N_2 loaded by C and R_c is

$$y_p = \frac{N_p}{D_p} \quad (23)$$

where

$$N_p = 1 - \omega^2 C \left(1 + \frac{1}{\omega^2 C^2 R_c^2} \right) (L_1 + L_2 + 2M) + j\omega C \left(1 + \frac{1}{\omega^2 C^2 R_c^2} \right) \left(R_1 + R_2 + \frac{R_c}{1 + \omega^2 C^2 R_c^2} \right) \quad (24)$$

and

$$D_p = R_2 - \omega^2 C \left(1 + \frac{1}{\omega^2 C^2 R_c^2} \right) \left[L_1 R_2 + L_2 \left(R_1 + \frac{R_c}{1 + \omega^2 C^2 R_c^2} \right) \right] \\ + j\omega L_2 \left[1 - \omega^2 C \left(1 + \frac{1}{\omega^2 C^2 R_c^2} \right) \left(L_1 - \frac{M^2}{L_2} \right) + \frac{C R_2}{L_2} \left(1 + \frac{1}{\omega^2 C^2 R_c^2} \right) \left(R_1 + \frac{R_c}{1 + \omega^2 C^2 R_c^2} \right) \right] \quad (25)$$

Component values for the quantities in circuit equations (2) and (22) to (25) were obtained for the commercial system. The connecting coaxial cable is approximately 35.6 meters (116 ft) long. Two electrically equivalent probes were measured: a cooled probe with a maximum tip temperature of 370°C (700°F), and an uncooled probe with a maximum tip temperature of 93°C (200°F). The probes were 9 millimeters ($3/8$ in.)

in diameter at the tip, were overall 80 millimeters (3 in.) long, and had a clearance range of 1000 micrometers (40 mils).

Values of the probe-tuning elements in equations (24) and (25) were derived from measurements of the terminal impedance of the probe using a Radiofrequency Vector Impedance Meter. A similar procedure was used to measure the values of the connecting coaxial cable parameters in equation (22). It is estimated that the impedance magnitude measurements have an accuracy of ± 10 percent and the phase angle measurements have an accuracy of $\pm 10^\circ$. These accuracies are adequate for the purposes of determining the change in the quantities outlined in the first paragraph of this section.

The source admittance y_g in equation (2) is $j\omega C_g$ where the source capacitance is designated C_g .

Component values and some of the resulting calculated quantities are as follows:

Electronics:

Source voltage, e_g , V	1.0
Source frequency, f , Hz	10.5×10^6
Source angular frequency, ω , rad/sec	66.0×10^6
Source capacitance, C_g , pF	47
Source admittance, y_g , S	$j3.1 \times 10^{-3}$
In-place recalibration admittance, y_k , S	$(0.73 + j2.3) \times 10^{-3}$

Coaxial cable:

Characteristic impedance, Z_0 , Ω	50.0
Attenuation constant times length, αl , neper	0.197
Phase constant times length, βl , rad	-0.490

Probe tuning elements:

Inductor L_1 , H	63×10^{-6}
Series resistance associated with L_1 , Ω	160
Inductor L_2 , H	0.46×10^{-6}
Series resistance associated with L_2 , Ω	0.1
Mutual inductance, M , H	3.38×10^{-6}

Probe tip:

Maximum expected ΔC , $(\Delta C)_m$, pF	0.21
Capacitance C over operating range of C_o , pF	4.30 to 4.36
Capacitance C over range of C that includes the operating range of C_o and all ΔC , pF	4.30 to 4.57
Minimum shunt resistance, R_c , Ω	1×10^6

The probe tip capacitances are approximate calculated values. They were determined from measurements of e made while varying the probe tip environment over the full temperature and humidity operating limits of the probe.

The curves of figures 10 and 11 are plots of the calculated magnitude and phase angle of e and y over the capacitance range of 3.5 to 5.5 picofarads for R_c much larger than the reactance of C and for R_c equal to its minimum value of 1 megohm. The curves of figure 12 are plots of the magnitude of $(de/dC)_0$ and $(dy/dC)_0$ over the operating range of C_0 (4.30 to 4.36 pF) for the same conditions of R_c .

It can be seen that the addition of the shunt resistance across C to the equivalent circuit has only minor influence on the curves over the region of interest near C_0 . The phase angle of e curve in figure 10 shows that this quantity changes slowly with C over the range of C which includes the operating range of C_0 and all ΔC . In the capacitance range of 4.30 to 4.57 picofarads the phase angle of e changes by less than 4° .

Examination of figure 12 shows that the magnitude of $(de/dC)_0$ is a strong function of C , while the magnitude of $(dy/dC)_0$ is a weaker function of C . Over the operating range of C_0 , the total change in $|(de/dC)_0|$ is 14 percent, and the total change in $|(dy/dC)_0|$ is only 3 percent. Thus $(dy/dC)_0$, which is used in the in-place recalibration technique, is clearly better than $(de/dC)_0$, which was used in the original system.

It is now shown that the tuning elements magnify the value of ΔC , causing y to be a sensitive indicator of clearance and minimizing the system's dependency on changes in coaxial cable parameters. If y were to be entirely capacitive, $|dy/dC|$ would equal ω or 66.0×10^6 . From figure 12, $|(dy/dC)_0|$ has a minimum value of 16.05×10^9 and therefore the value of ΔC is magnified by the ratio $16.05 \times 10^9 / 66.0 \times 10^6$ or approximately 240. Thus the $(\Delta C)_m$ of 0.21 picofarad is equivalent to a change of approximately 50 picofarads at the input terminal. Besides providing a larger change in voltage e , the use of tuning elements also minimizes dependency on changes in coaxial cable parameters, since the small changes in the coaxial cable reactance elements due to motion and vibration are now compared with 50 picofarads rather than 0.21 picofarad.

EXPERIMENTAL DATA USING THE IN-PLACE RECALIBRATION TECHNIQUE

The in-place recalibration technique was applied to the commercial system described in the previous section under separate conditions of extreme temperature and humidity. Two electrically equivalent probes were measured: one, a cooled, 370°C (700°F) type; the other, an uncooled, 93°C (200°F) type. Heaters were used to raise the probe tip from room temperature to the maximum allowed temperature for each type. A humidity enclosure provided the probe-tip environment which was varied over its full operating limits of 5 percent to 95 percent relative humidity at room temperature. The values of $\Delta |e_y|$ were obtained by using the calibration system of figure 6 and the measurement methods described in an earlier section. The quantity $\Delta |e_{ya}|$ corresponds to the ambient condition found at calibration. The quantity $\Delta |e_{yb}|$

was obtained at the extreme environmental condition of the test. Equation (19) was used to correct the data.

The data points of figure 13 are the errors in clearance before and after correction as a function of clearance over the operating limits of 5 to 95 percent relative humidity at room temperature. For each clearance the data point is the worst error out of four measurements taken. Over the range of 0 to 1000 micrometers (40 mils) the in-place recalibration technique reduced the maximum error caused by changes in humidity from 45 micrometers (1.8 mils) to 10 micrometers (0.4 mil).

The data points of figure 14 are the errors in clearance before and after correction as a function of clearance over the operating limits of room temperature to the maximum allowed temperature. As before, the data point is the worst error for that clearance. Over the range of 0 to 1000 micrometers (40 mils) the in-place recalibration technique reduced the maximum error caused by changes in temperature from 88 micrometers (3.5 mils) to 40 micrometers (1.6 mils). The larger errors, after correction in the maximum allowed temperature environment as compared with the humidity case, are probably due to local heating of the tuning elements.

SUMMARY OF RESULTS

The rotor-blade-tip clearance system consists of a capacitance-sensing probe with self-contained tuning elements, a connecting coaxial cable, and remote electronics. Tests showed that the accuracy of the system suffered from a strong dependence on probe temperature and humidity. An in-place recalibration technique was presented which partly overcame this problem through a simple modification of the electronics that permitted an in-place scale-factor correction. When this technique was applied to a commercial system, significant reductions in the errors under conditions of varying humidity and temperatures were demonstrated. Equations were also found that characterized the important cable and probe design quantities.

Lewis Research Center,
National Aeronautics and Space Administration,
Cleveland, Ohio, January 23, 1978,
505-04.

APPENDIX A

CABLE AND PROBE DESIGN

In this appendix equations are derived that characterize the important cable and probe design quantities. It is shown that

(1) For long distances between the probe and the electronics, the input admittance of the probe may require scaling.

(2) The scaling of y_p can be achieved by mutual coupling between inductive tuning elements of the probe.

(3) The connecting coaxial cable must be taken into consideration in any system design.

From transmission line theory (ref. 2), it is known that

$$y = \frac{1}{Z_0} \left[\frac{y_p Z_0 + \tanh(\alpha + j\beta)l}{1 + y_p Z_0 \tanh(\alpha + j\beta)l} \right] \quad (A1)$$

where Z_0 is the characteristic impedance, α is the attenuation constant, β is the phase constant, and l is the length of the line.

In the conventional application of transmission lines, the cable is terminated by the fixed resistance Z_0 , which results in a y of $1/Z_0$. For the present application, however, it is necessary that y be a function of y_p . If the distance between the probe tip and the electronics is very short, then from equation (A1) $y = y_p$ since l in effect is equal to zero. On the other hand, when the distance is long, neither the simultaneous inequalities

$$\left. \begin{aligned} y_p Z_0 &\gg \tanh(\alpha + j\beta)l \\ 1 &\ll y_p Z_0 \tanh(\alpha + j\beta)l \end{aligned} \right\} \quad (A2)$$

nor the simultaneous inequalities

$$\left. \begin{aligned} y_p Z_0 &\ll \tanh(\alpha + j\beta)l \\ 1 &\gg y_p Z_0 \tanh(\alpha + j\beta)l \end{aligned} \right\} \quad (A3)$$

are permitted for y to be a function of y_p . It is clear that if both inequalities of (A2) or of (A3) are satisfied, y no longer depends on y_p . Neither the simultaneous inequalities of (A2) nor of (A3) are satisfied if the relationship expressed loosely by

$$y_p \approx \frac{1}{Z_0} \quad (\text{A4})$$

is met. Further, the equality

$$1 = \tanh(\alpha + j\beta)l \quad (\text{A5})$$

that is, the simultaneous equalities

$$\left. \begin{aligned} 1 &= \frac{\tanh \alpha l (1 + \tan^2 \beta l)}{1 + \tanh^2 \alpha l \tan^2 \beta l} \\ 0 &= \frac{\tan \beta l (1 - \tanh^2 \alpha l)}{1 + \tanh^2 \alpha l \tan^2 \beta l} \end{aligned} \right\} \quad (\text{A6})$$

is not permitted if y is to be a function of y_p . The equalities of (A6) cannot be simultaneously satisfied because the function $\tanh \alpha l$ has a value less than 1.0 for finite αl . Thus, the approximation of (A4) is the only requirement for y to be a function of y_p .

For any given probe network N_2 , y_p may be relatively fixed and therefore may be unable to meet the approximation of (A4). Thus, the network for N_2 must demonstrate a feature such as simple scaling of y_p to achieve the desired approximation.

A commonly used tuning circuit which will ultimately lead to the network of figure 9 is now analyzed. It is shown that for a number of practical reasons y_p is indeed relatively fixed for the network and cannot be scaled in its present form. Figure 15 is the circuit for N_2 loaded by C . For the present discussion the shunt resistance across the capacitance and the series resistances associated with the inductors are neglected. This can be done since radiofrequency circuits are usually designed to have large reactances compared with their resistances. A series resonant circuit is formed by L_a and C , while the parallel combination of L_b and the series circuit is another resonant circuit. The resultant input admittance has no real part, while its imaginary part, called the input susceptance B_o , is written as

$$B_o = \frac{1 - \omega^2 C(L_a + L_b)}{-\omega L_b + \omega^3 C L_a L_b} = \frac{1 - \omega^2 C(L_a + L_b)}{-\omega L_b (1 - \omega^2 C L_a)} \quad (\text{A7})$$

In network theory one often deals with the susceptance as a function of frequency. The undamped natural frequencies, called critical frequencies, are important design

quantities. Because capacitance rather than frequency is the variable of interest here, a set of analogous critical capacitances are sought. The critical capacitances are defined in terms of the positive roots of the numerator and denominator of susceptance. The capacitance that makes the numerator zero shall be called a capacitance zero, and the capacitance that makes the denominator zero shall be called a capacitance pole. Thus for B_0 from equation (A7)

$$C_{zo} = \frac{1}{\omega^2(L_a + L_b)} \quad (A8)$$

is the probe capacitance zero and

$$C_{po} = \frac{1}{\omega^2 L_a} \quad (A9)$$

is the probe capacitance pole.

As mentioned in an earlier section, the value of C_0 depends on the geometry of the coaxial probe tip and the dielectric properties of the insulator. The diameter of the probe tip is usually determined by the range of the clearance; that is, the higher the range, the larger the diameter. The tip is made long enough to reach inside the shroud of the rotor stage to be measured. Thus, the design of the probe tip and therefore the value of C_0 is relatively fixed for any given installation. For high system sensitivity the change in B_0 should be a strong function of the change in C at $C = C_0$. This means that the derivative of B_0 with respect to C evaluated at $C = C_0$ should be large. Using equations (A7) and (A9) the derivative is given by

$$\left. \frac{dB_0}{dC} \right|_{C=C_0} = \frac{\omega}{(1 - \omega^2 C_0 L_a)^2} = \frac{\omega}{\left(1 - \frac{C_0}{C_{po}}\right)^2} \quad (A10)$$

For a given ω , $\left. dB_0/dC \right|_{C=C_0}$ is largest when C_{po} is of the same order of magnitude as C_0 . Since C_0 is relatively fixed, then C_{po} is also relatively fixed. The minimum ω is determined by the required speed of response. Long transmission line lengths and electronic equipment considerations place an upper limit on ω . Within the practical range of ω , determination of L_a from equation (A9) results in a relatively large value for a radiofrequency inductor. Since the same constraint applies to L_b in equation (A8), C_{zo} is of the same order of magnitude as C_{po} . Thus, for a given installation the

values of L_a , L_b , C , and B_o in figure 15 are relatively fixed. But because equation (A4) demands that B_o be approximately $1/Z_o$, it may be necessary to scale B_o .

The following synthesis shows that the scaling of B_o can be achieved through the addition of mutual coupling of the inductive tuning elements. Figure 16 is the same as figure 15 except that mutual coupling has been added. The input susceptance B_p is now written as

$$B_p = \frac{1 - \omega^2 C(L_1 + L_2 + 2M)}{-\omega L_2 + \omega^3 C(L_1 L_2 - M^2)} \quad (\text{A11})$$

where the sign of M is taken in the dot convention shown in figure 16. If B_o is to be scaled by $1/k$ where k is real and positive then the equality

$$\frac{B_o}{k} = B_p \quad (\text{A12})$$

must be met. Figure 16 represents a physically realizable network synthesis of B_p satisfying equation (A12) if the element values L_1 , L_2 , and M are physically realizable for all k . Thus, L_1 and L_2 must be real and positive and M must be real and satisfy then inequality

$$L_1 L_2 - M^2 > 0 \quad (\text{A13})$$

Using equations (A7) and (A11), equation (A12) can be written

$$\frac{1 - \omega^2 C(L_a + L_b)}{-\omega k L_b + \omega^3 C k L_a L_b} = \frac{1 - \omega^2 C(L_1 + L_2 + 2M)}{-\omega L_2 + \omega^3 C(L_1 L_2 - M^2)} \quad (\text{A14})$$

A solution of equation (A14) may be found by equating coefficients of corresponding powers of ω in the numerator and denominator. Performing this operation yields the equations

$$L_a + L_b = L_1 + L_2 + 2M \quad (\text{A15})$$

$$k L_b = L_2 \quad (\text{A16})$$

$$kL_a L_b = L_1 L_2 - M^2 \quad (\text{A17})$$

By solving equations (A15) to (A17) simultaneously, L_1 and M become

$$L_1 = L_a + \frac{M^2}{kL_b} \quad (\text{A18})$$

$$M = -L_b(k \pm \sqrt{k}) \quad (\text{A19})$$

The $-\sqrt{k}$ is chosen for convenience since for $k = 1$, $M = 0$, and the circuit of figure 16 reduces to 15. In summary

$$L_1 = L_a + L_b(\sqrt{k} - 1)^2 \quad (\text{A20})$$

$$L_2 = kL_b \quad (\text{A21})$$

$$M = -L_b \sqrt{k}(\sqrt{k} - 1) \quad (\text{A22})$$

It is clear that L_1 and L_2 are real and positive and that M is real and, by equation (A17), satisfies (A13). Thus, the synthesis is valid and the scaling of B_0 can be achieved through the addition of mutual coupling between the inductive tuning elements.

To find the critical capacitances for figure 16, equation (A11) is rewritten as

$$B_p = \frac{1 - \omega^2 C(L_1 + L_2 + 2M)}{-\omega L_2 \left[1 - \omega^2 C \left(L_1 - \frac{M^2}{L_2} \right) \right]} \quad (\text{A23})$$

The probe capacitance zero and the probe capacitance pole are therefore

$$C_{zp} = \frac{1}{\omega^2(L_1 + L_2 + 2M)} \quad (\text{A24})$$

and

$$C_{pp} = \frac{1}{\omega^2 \left(L_1 - \frac{M^2}{L_2} \right)} \quad (\text{A25})$$

In this discussion the shunt resistance across the capacitance and the series resistance associated with the inductors were neglected. Figure 9 is the same as figure 16 except that the resistances have been included.

Equations (A24) and (A25) are expressions for the capacitance zero and the capacitance pole of the probe circuit. It is of some interest to determine the critical capacitances for the input admittance of the connecting coaxial cable loaded by the probe as shown in figure 4. The input susceptance part of y in equation (A1) with $y_p = jB_p$ and $\alpha = 0$ can be written in the form

$$B = \frac{\left(1 - \frac{\omega L_2 \tan \beta l}{Z_0} \right) - \frac{C}{C_{zp}} \left(1 - \frac{C_{zp}}{C_{pp}} \cdot \frac{\omega L_2 \tan \beta l}{Z_0} \right)}{-\omega L_2 \left\{ \left(1 + \frac{Z_0 \tan \beta l}{\omega L_2} \right) - \frac{C}{C_{pp}} \left[1 + \frac{C_{pp}}{C_{zp}} \cdot \frac{Z_0 \tan \beta l}{\omega L_2} \right] \right\}} \quad (\text{A26})$$

As before, the critical capacitances are defined in terms of the positive roots of the numerator and denominator of the susceptance. The capacitance zero and the capacitance pole of the cable loaded by the probe are therefore

$$C_z = C_{zp} \cdot \frac{1 - \frac{\omega L_2 \tan \beta l}{Z_0}}{1 - \frac{C_{zp}}{C_{pp}} \cdot \frac{\omega L_2 \tan \beta l}{Z_0}} \quad C_z > 0 \quad (\text{A27})$$

and

$$C_p = C_{pp} \cdot \frac{1 + \frac{Z_0 \tan \beta l}{\omega L_2}}{1 + \frac{C_{pp}}{C_{zp}} \cdot \frac{Z_0 \tan \beta l}{\omega L_2}} \quad C_p > 0 \quad (\text{A28})$$

Examination of equations (A27) and (A28) reveals that the probe critical capacitances may be shifted or may disappear when they are observed from the input of the connecting coaxial cable. Thus, the connecting coaxial cable must be taken into consideration in any system design.

For the commercial system the various critical capacitances and the operating range of C_o are as follows:

Probe:

$$\text{Operating range of } C_o = 4.30 \times 10^{-12} \text{ to } 4.36 \times 10^{-12} \text{ F}$$

$$C_{zp} = 3.27 \times 10^{-12} \text{ F}$$

$$C_{pp} = 6.02 \times 10^{-12} \text{ F}$$

Cable loaded by the probe:

$$C_z = 3.68 \times 10^{-12} \text{ F}$$

C_p does not exist

The operating range of C_o lies between C_{zp} and C_{pp} and above C_z . The operating range of C_o and C_z are indicated in figure 11, which is the calculated magnitude and phase angle of y . Note that C_z is a good approximation of the value of C for which the magnitude of y is a minimum and the phase angle of y is zero.

APPENDIX B

SYMBOLS

A	amplitude detector
B	input susceptance part of y , S
B_o	input susceptance in fig. 15, S
B_p	input susceptance part of y_p , S
C	capacitance, F
ΔC	$C_m - C_o$, F
C(d)	blade capacitance, F
C(t)	capacitance as a function of time, F
C_g	source capacitance, F
C_m	total capacitance at point of maximum capacitance, $C_m = C_o + C(d)$, F
$(\Delta C)_m$	maximum expected ΔC , F
C_o	coaxial-probe-tip capacitance, F
C_p	capacitance pole of B, F
C_{po}	capacitance pole of B_o , F
C_{pp}	capacitance pole of B_p , F
C_z	capacitance zero of B, F
C_{zo}	capacitance zero of B_o , F
C_{zp}	capacitance zero of B_p , F
D_p	denominator of y_p , eq. (23)
d	clearance, μm
e	voltage, V
e_c	e when C is changed, V
$\Delta e_c $	change in magnitude of e_c , V
$e_{cm} - e_{co}$	change of e_c as result of change in capacitance, $C_m - C_o$, V
e_{co}	e_c for $C = C_o$, V
e_g	source voltage, V
e_y	e when y is changed, V

$\Delta e_y $	change in magnitude of e_y , V
$e_{yn} - e_{yo}$	change in e_y as the result of change in admittance $y_n - y_o$, V
e_{yo}	e_y for $C = C_o$ with switch K open, V
f	source frequency, Hz
$j\omega$	variable
K	in-place recalibration switch
K_{1C}, K_{2C}, \dots	coefficients of nonlinear approximation (eq. (20))
K_{1y}, K_{2y}, \dots	coefficients of nonlinear approximation (eq. (21))
k	real and positive constant, $B_o/k = B_p$
L_a, L_b	probe-tuning inductors in fig. 15, H
L_1, L_2	probe-tuning inductors in figs. 9 and 16, H
l	length
M	probe-tuning mutual inductance, H
N	cable and probe-tuning elements network
N_p	numerator of y_p , eq. (23)
N_1	cable network
N_2	probe-tuning elements network
R_c	shunt resistance, Ω
R_1, R_2	series resistances associated with L_1 and L_2 , respectively, Ω
y	admittance, S
y_g	source admittance, S
y_k	in-place recalibration admittance, S
y_n	y for $C = C_o$ with switch K closed, $y_n = y_o + y_k$, S
y_o	y for $C = C_o$ with switch K open, S
y_p	probe admittance, S
Z_0	coaxial cable characteristic impedance, Ω
α	coaxial cable attenuation constant, nepers/unit length
β	coaxial cable phase constant, rad/unit length
ω	source angular frequency, rad/sec

Subscripts:

- a calibration condition
- b operational condition



REFERENCES

1. Oliver, Frank J.: Practical Instrumentation Transducers. Hayden Book Company, 1971, p. 20.
2. Reference Data for Radio Engineers. Sixth ed., Howard W. Sams & Co., 1975, p. 24-4.

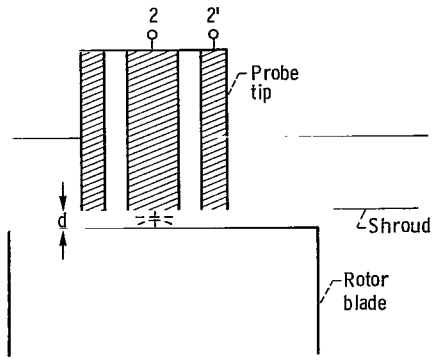


Figure 1. - Schematic of rotor blade and probe tip of typical shroud mounted capacitance-sensing probe.

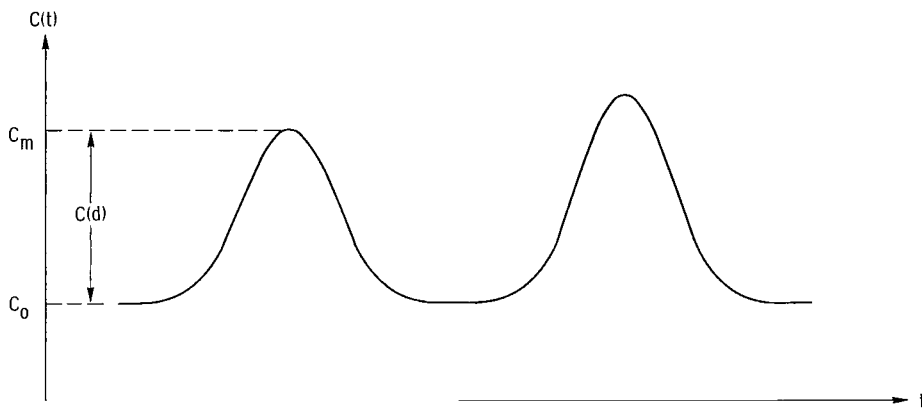


Figure 2. - Capacitance as function of time for passing of two blades under probe tip.

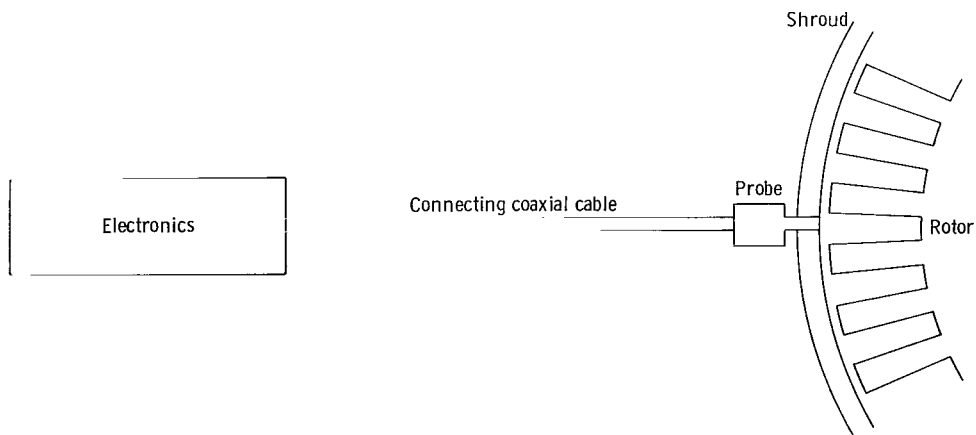


Figure 3. - System block diagram.

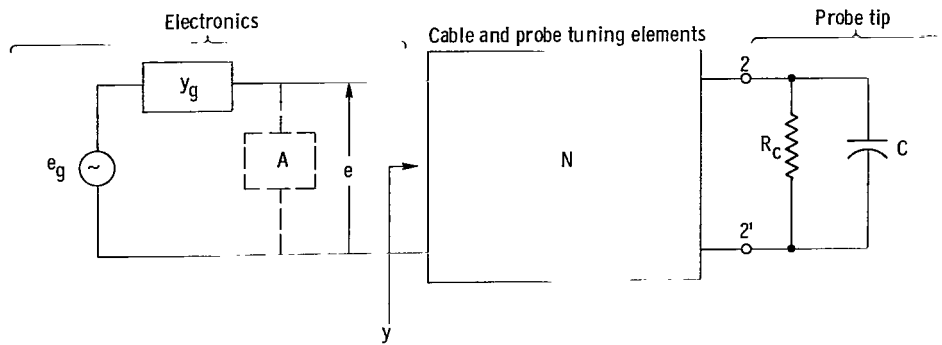


Figure 4. - System equivalent circuit.

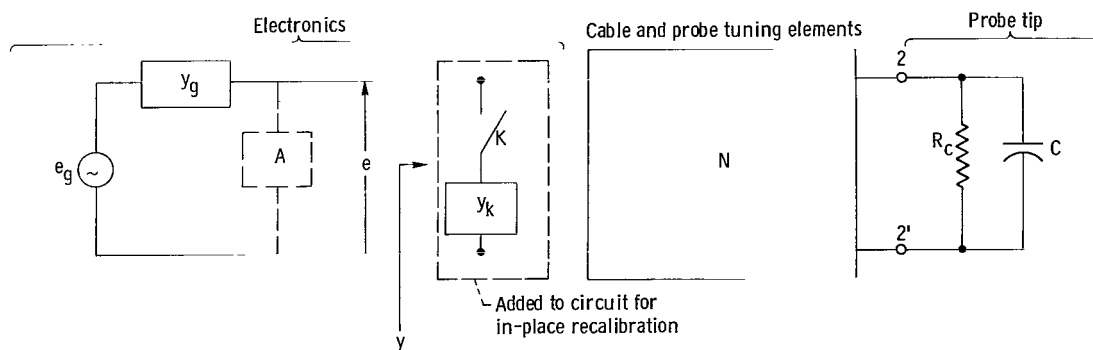


Figure 5. - System equivalent circuit with in-place recalibration.

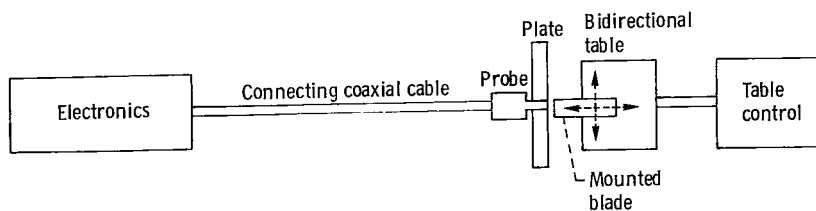


Figure 6. - Block diagram of calibration system.

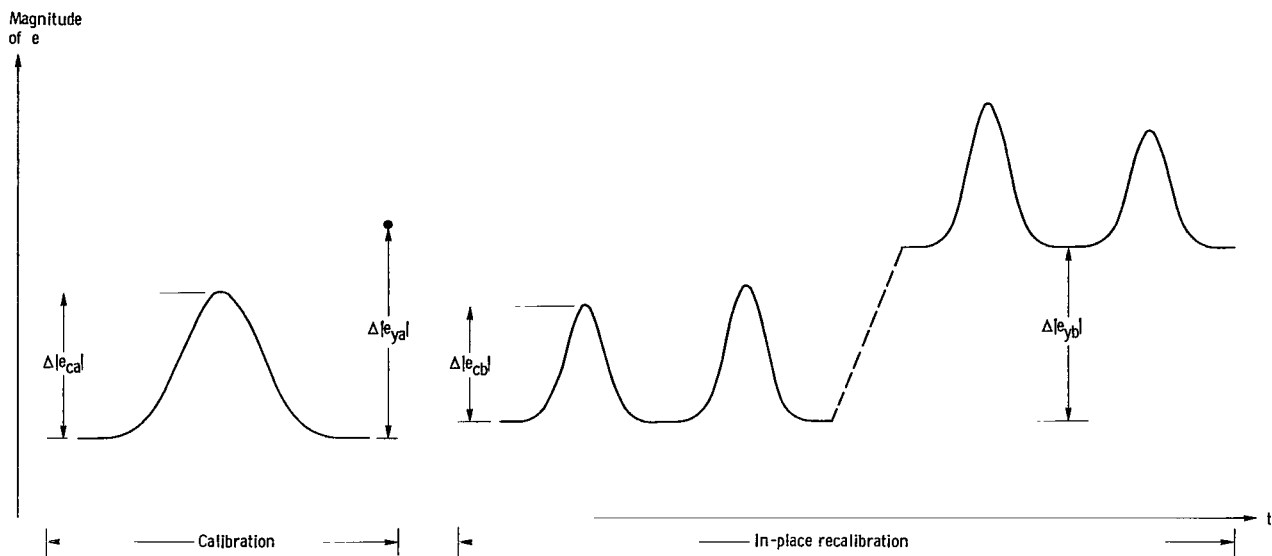


Figure 7. - Output of amplitude detector during calibration and in-place recalibration. (Time axis t is not to scale.)

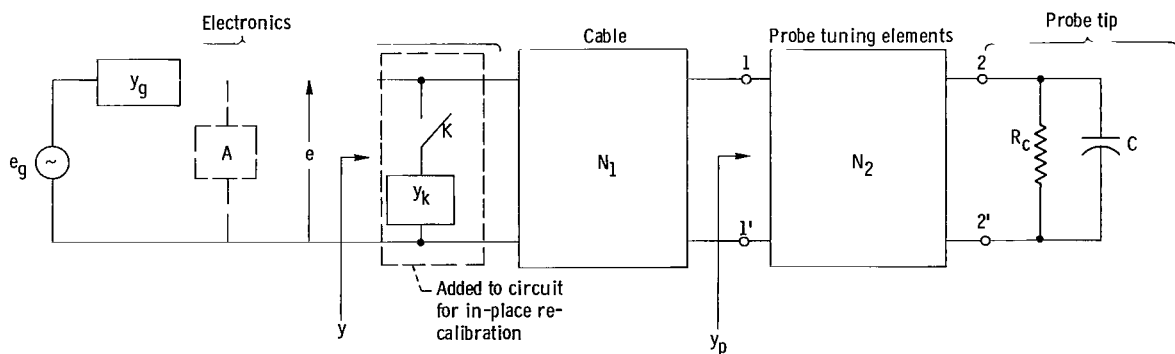


Figure 8. - System equivalent circuit with in-place recalibration. Network N is separated into two networks, N_1 for the cable and N_2 for the probe tuning elements.

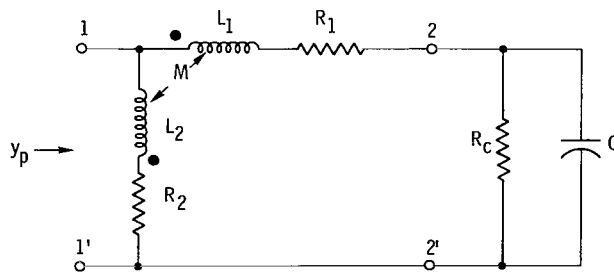


Figure 9. - Circuit for N_2 loaded by C and R_c with mutual coupling.

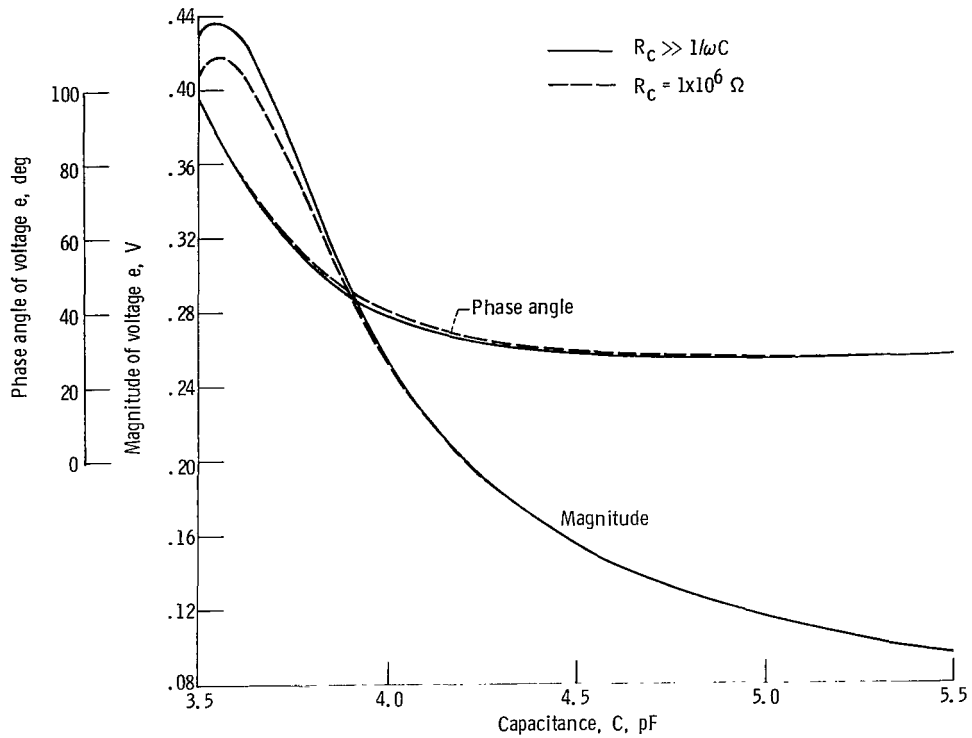


Figure 10. - Calculated magnitude and phase angle of e over capacitance range of 3.5 to 5.5 picofarads.

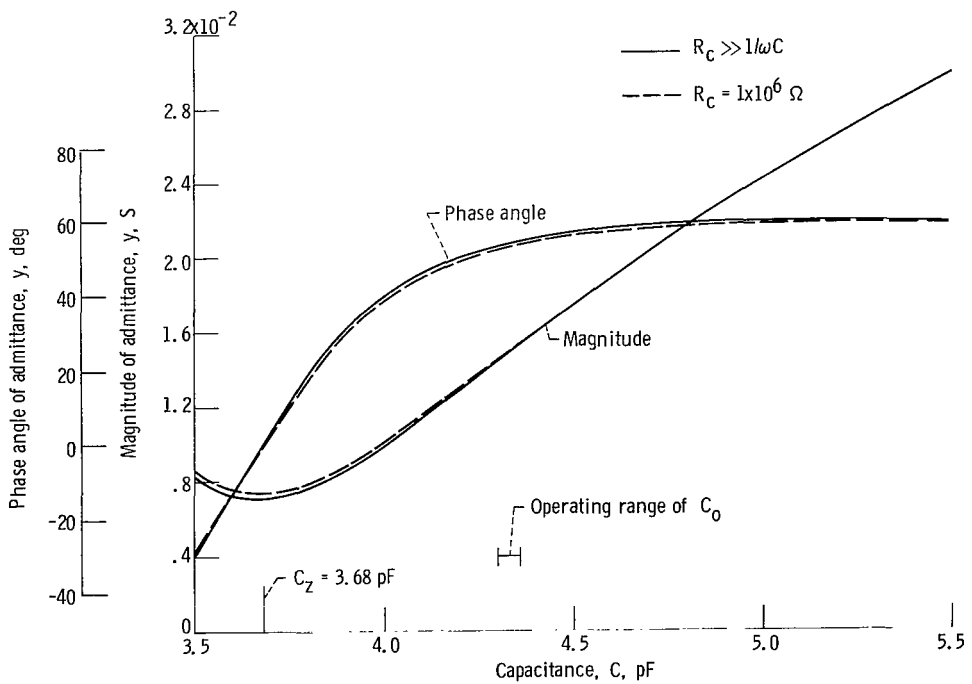


Figure 11. - Calculated magnitude and phase angle of y over capacitance range of 3.5 to 5.5 picofarads.

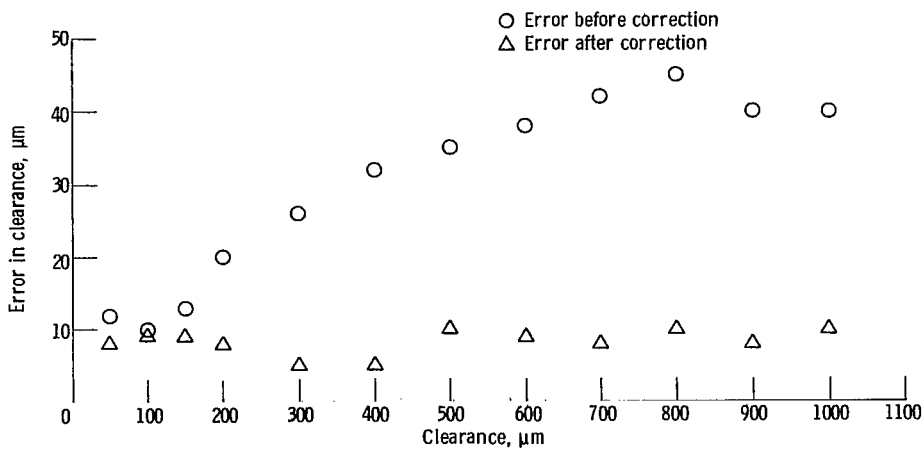


Figure 13. - Errors in clearance before and after correction as function of clearance over operating limits of 5 to 95 percent relative humidity at room temperature.

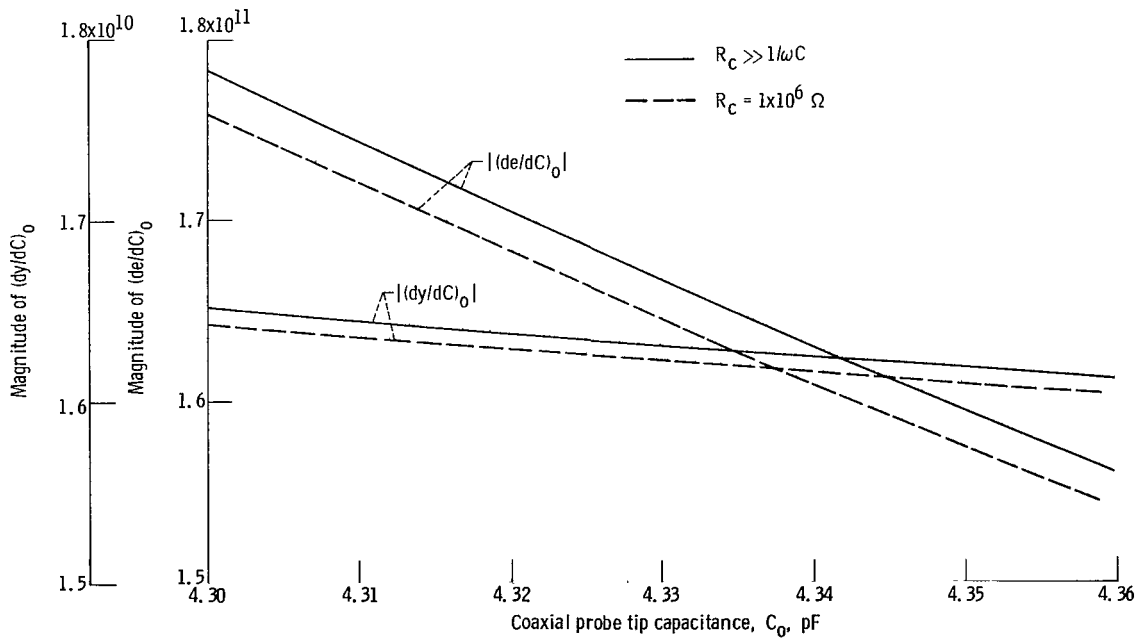


Figure 12. - Calculated magnitude of $(de/dC)_0$ and $(dy/dC)_0$ over operating range of C_0 .

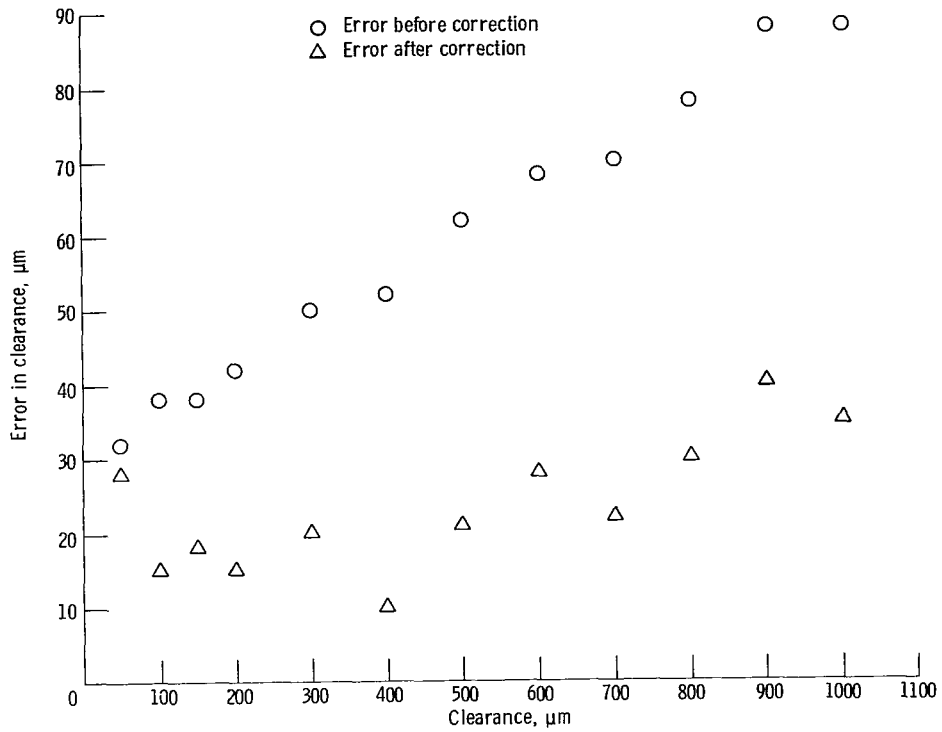


Figure 14. - Errors in clearance before and after correction as function of clearance over operating limits of room temperature to maximum allowed temperature (370° C (700° F) for cooled probe and 93° C (200° F) for the uncooled probe).

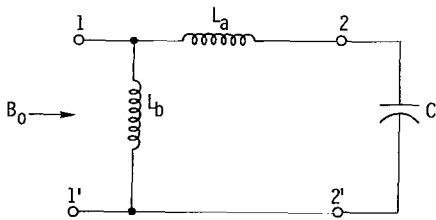


Figure 15. - Circuit for N_2 loaded by C neglecting all resistances.

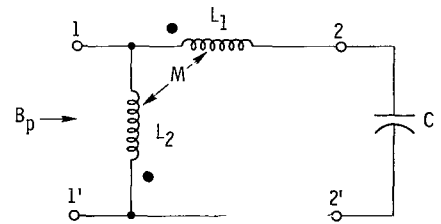


Figure 16. - Circuit for N_2 loaded by C with mutual coupling neglecting all resistances.

1. Report No. NASA TP-1110	2. Government Accession No.	3. Recipient's Catalog No.
4. Title and Subtitle IN-PLACE RECALIBRATION TECHNIQUE APPLIED TO A CAPACITANCE-TYPE SYSTEM FOR MEASURING ROTOR BLADE TIP CLEARANCE	5. Report Date April 1978	6. Performing Organization Code
7. Author(s) John P. Barranger	8. Performing Organization Report No. E-9395	10. Work Unit No. 505-04
9. Performing Organization Name and Address National Aeronautics and Space Administration Lewis Research Center Cleveland, Ohio 44135	11. Contract or Grant No.	13. Type of Report and Period Covered Technical Paper
12. Sponsoring Agency Name and Address National Aeronautics and Space Administration Washington, D. C. 20546	14. Sponsoring Agency Code	
15. Supplementary Notes		
16. Abstract The rotor-blade-tip clearance measurement system consists of a capacitance-sensing probe with self-contained tuning elements, a connecting coaxial cable, and remotely located electronics. Tests show that the accuracy of the system suffers from a strong dependence on probe tip temperature and humidity. A novel in-place recalibration technique is presented which partly overcomes this problem through a simple modification of the electronics that permits a scale factor correction. This technique, when applied to a commercial system, significantly reduced errors under varying conditions of humidity and temperature. Equations are also found that characterize the important cable and probe design quantities.		
17. Key Words (Suggested by Author(s)) Instrumentation; Nondestructive testing; Blade tips; Clearances; Capacitance; Jet engines; Engine diagnostics; Sensors and transducers; Circuitry; Calibration; Turbomachinery	18. Distribution Statement Unclassified - unlimited STAR Category 07	
19. Security Classif. (of this report) Unclassified	20. Security Classif. (of this page) Unclassified	21. No. of Pages 33
		22. Price* A03

National Aeronautics and
Space Administration

Washington, D.C.
20546

Official Business
Penalty for Private Use, \$300

THIRD-CLASS BULK RATE

Postage and Fees Paid
National Aeronautics and
Space Administration
NASA-451



1 1 1U,A, 041978 S00903DS
DEPT OF THE AIR FORCE
AF WEAPONS LABORATORY
ATTN: TECHNICAL LIBRARY (SUL)
KIRTLAND AFB NM 87117

NASA

POSTMASTER: Not Deliverable (Section 158
Postal Manual) Do Not Return